e-Prime - Advances in Electrical Engineering, Electronics and Energy 2 (2022) 100039

Contents lists available at ScienceDirect

e-Prime - Advances in Electrical Engineering, Electronics and Energy

journal homepage: www.elsevier.com/locate/prime

A novel improved version of hunger games search algorithm for function optimization and efficient controller design of buck converter system

Davut Izci [a,*], Serdar Ekinci [b]

[a] Department of Electronics & Automation, Batman University, Batman, 72060 Turkey
[b] Department of Computer Engineering, Batman University, Batman, 72100, Turkey

ARTICLE INFO

Keywords:
Hunger games search
Nelder-Mead simplex method
Random learning mechanism
Fractional-order PID controller
Buck converter system

ABSTRACT

There is a continuous effort to develop efficient control mechanisms for power converters as it is a challenging task due to nonlinear nature of such systems. As part of the ongoing effort in the related field, a novel control method is presented in this paper. The proposed method with this study involves a fractional order proportional-integral-derivative (FOPID) controller and the development of a novel metaheuristic algorithm for tuning in order to achieve optimum performance of a buck converter system. In terms of the metaheuristic algorithm, an improved version of the hunger games search (IHGS) algorithm is developed by enhancing the intensification and the diversification abilities of the hunger games search (HGS) algorithm with the aid of Nelder-Mead simplex method and the random learning mechanism, respectively. Several classical unimodal, multimodal, and fixed dimensional benchmark functions along with CEC2019 test suite are used to confirm the improved structure of the developed IHGS algorithm. A novel objective function is also constructed in this study by modifying the structure of the performance index known as integral of squared error. The novel IHGS algorithm together with the novel objective function are proposed as an efficient tool to design a FOPID controller employed in a buck converter system. The proposed method's superiority for the operation of a buck converter system is confirmed comparatively with transient and frequency responses along with robustness analysis in terms of parametric uncertainties and measurement noise along with input and load voltage fluctuations using the best performing methods of artificial ecosystem optimization algorithm based PID, Lévy flight distribution algorithm based PIDA and Harris hawks optimization algorithm based FOPID controllers. The other capable approaches reported in the literature are also used to further confirm the excellent ability of the proposed method for controlling a buck converter system.

1. Introduction

A buck converter system is an electronic circuit that is popular for decreasing and regulating the output voltage. The popularity of this type of DC-DC power converter stems from its lower cost, less complexity, easier implementation and good performance [1]. The control of such power converters is not only challenging but also a crucial task due to their wider utilization in many applications for regulating the voltage at a desired level [2]. The main challenge arises from the nonlinear structures of such systems which makes it difficult to design a stable and robust controller as they are susceptible to input and parametric changes greatly [3]. Therefore, the researchers in the field have paid a significant attention to the control of such converters for the past few decades [4].

In terms of the controllers, one must consider the stability and the robustness. In the meantime, tracking accuracy, transient and frequency response characteristics of the controlled system must also be satisfied. In this regard, an extensive research has been performed to design the controllers with the stated features for DC-DC power converters [5]. To achieve a stable operation for the DC-DC power converters, different controller types such as proportional-integral-derivative (PID) [6], PID and acceleration (PIDA) [7], fractional order PID (FOPID) [8], adaptive [9], sliding mode [10] and model predictive [11] controllers have so far been proposed.

Amongst those controllers, the PID controller has a wider employment due to its relatively easier implementation, simple structure and yet good ability [6]. Despite the latter listed advantages, a PID controller is not the best suitable option for practical cases where nonlinearities, disturbances and parametric variations exist [12]. Therefore, there has

* Corresponding author.
E-mail addresses: davut.izci@batman.edu.tr (D. Izci), serdar.ekinci@batman.edu.tr (S. Ekinci).

https://doi.org/10.1016/j.prime.2022.100039
Received 13 April 2022; Accepted 18 April 2022
Available online 20 April 2022
2772-6711/© 2022 The Author(s). Published by Elsevier Ltd. This is an open access article under the CC BY-NC-ND license (http://creativecommons.org/licenses/by-nc-nd/4.0/).

been a significant interest in the fractional counterpart (FOPID) of the PID controllers in the past few decades considering the latter disadvantage [13]. Similar to other fractional order systems [14], a FOPID controller also adopts non-integer integrals and derivatives providing a significant robustness to disturbances, parameter variations and uncertainties [15]. Because a FOPID controller is an extension of a PID controller with two additional parameters providing an increased degree of freedom and making it more flexible for design requirements [13]. The above-mentioned features allow the FOPID controllers to perform with better efficiency in terms of controlling nonlinear systems such as the power converters [16]. Therefore, this study employs a FOPID controller to operate a DC-DC buck converter system efficiently.

Meanwhile, the parameters of the FOPID controller needs to be tuned appropriately [17] in order to fully benefit from its flexibility for efficient operation of DC-DC power converters [18]. In this regard, the metaheuristic optimization algorithms play a key role regardless of the type of controller being used [6–8]. The related studies of metaheuristic algorithms-based design approaches have so far shown their excellent capacity for efficient operation of the power converters. Based on this fact, this paper attempts to demonstrate a novel approach to allow more efficient operation of a buck converter. Therefore, a novel metaheuristic algorithm is proposed in this study. In that respect, the capability of a recently proposed metaheuristic algorithm named hunger games search (HGS) algorithm [19] is improved with the appropriate aid of Nelder-Mead simplex (NMS) method [20] and random learning mechanism (RLM) [21]. In here, NMS is used to allow further intensification and the RLM is adopted for further diversification. The proposed improved HGS (IHGS) algorithm is used as a more efficient tool to design a FOPID controller employed in a buck converter system. Apart from a novel metaheuristic algorithm, this study also proposes a novel objective function to achieve optimal parameters of the FOPID controller employed in the buck converter system. For the latter purpose, a modified version of the performance index, named integral of squared error [7], is used. The proposed novel objective function is minimized to reach better transient performance metrics. The following list can be used to sum up the main contributions of this work:

- A novel improved version of the HGS (IHGS) algorithm is developed with the aid of NMS and RLM techniques in order to achieve better intensification and diversification.
- The proposed IHGS algorithm is confirmed for its excellent capability through testing it against twenty-three well-known classical unimodal, multimodal, fixed-dimensional benchmark functions and challenging CEC2019 test suite comparatively.
- The novel IHGS algorithm is proposed as an efficient design tool for a FOPID controller adopted in a DC-DC buck converter system.
- To reach optimal parameters of the FOPID controller, a novel objective function is also proposed.
- The excellent performance of the proposed approach is demonstrated comparatively through transient and frequency responses along with robustness for parameter uncertainties and measurement noise along with input and load voltage fluctuations using the best performing methods of Harris hawks optimization algorithm based FOPID controller [18], Levy flight distribution algorithm based PIDA controller [7] and artificial ecosystem optimization algorithm based PID controller [6].
- The proposed method is also confirmed to be an excellent technique by performing a comparative analysis using other best performing and available approaches reported for the same buck converter system in the literature [6–8,18,22–24].

The organization of this paper is as follows. Section 2 provides details on HGS algorithm whereas Section 3 presents the proposed IHGS algorithm and the aiding structures of NMS and RLM. The experimental results for demonstration of the intensification and diversification of the proposed IHGS algorithm is discussed in Section 4. The detailed model of the buck converter system is presented in Section 5. The following section explains the FOPID controlled buck converter system and Section 7 describes the proposed novel method to achieve an optimal design. Section 8 provides the comparative transient, frequency and robustness analyses and Section 9 concludes the paper.

2. Hunger games search algorithm

The survival of the animals in nature depends on their hunger-driven activities. In that respect, the decisions on their motions play a significant role in terms of survival. The hunger games search (HGS) algorithm considers the latter reality and mathematically models the hunger-driven activities and behavioral choices as a set of game rules [19] such that it can be used as an efficient metaheuristic optimization tool. The game rule mimics cooperation between the animals during foraging. However, it also considers the reluctance of the individuals for such a cooperation, as well. This game rule can be represented as follows:

$$\overline{X(t+1)} = \begin{cases} Game_1 : \overline{X(t)} \cdot (1 + randn(1)), \ r_1 < C \\ Game_2 : \overline{W_1} \cdot \overline{X_b} + \overline{R} \cdot \overline{W_2} \cdot |\overline{X_b} - \overline{X(t)}|, \ r_1 > C, \ r_2 > E \\ Game_3 : \overline{W_1} \cdot \overline{X_b} - \overline{R} \cdot \overline{W_2} \cdot |\overline{X_b} - \overline{X(t)}|, \ r_1 > C, \ r_2 < E \end{cases} \quad (1)$$

where, r_1 and r_2 are two random numbers within $[0, 1]$ whereas $randn(1)$ is another random number satisfying normal distribution. On the other hand, t stands for the current iteration, $\overline{W_1}$ and $\overline{W_2}$ represent the hunger weights, $\overline{X_b}$ denotes the location of the best individual and $\overline{X(t)}$ stands for the location of each individual in current iteration. The choice between the designated rules ($Game_1$, $Game_2$ and $Game_3$) are determined based on the parameter of C. The parameter of $\overline{R}$ is calculated as $\overline{R} = 2 \times shr \times rand - shr$ where $shr = 2 \times (1 - (t/T))$. In the latter definition, $rand$ stands for a random number within $[0, 1]$ and T represents the maximum number of iterations. The variations of all positions are controlled with E parameter which is defined as $E = sech(|F(i) - BFit|)$ where $F(i)$ is the fitness value of each individual, $BFit$ is of the best one obtained so far and $i \in 1, 2, \ldots, n$. $sech$ represents a hyperbolic function and calculated as $sech(x) = (2/(e^x + e^{-x}))$. Considering the general structure explained by Eq. (1), it is feasible to talk about two search categories. The first one represents the self-dependent individuals whereas the second one simulates the teamwork. In this way, the individuals can reach an increased diversification.

The starvation characteristics of each individual is also mimicked by the HGS algorithm. The hunger weights given in Eq. (1) can be expressed as follows where N represents the number of individuals and $Shng$ denotes the sum of hungry feelings of all individuals.

$$\overline{W_1(i)} = \begin{cases} hng(i) \cdot \dfrac{N}{Shng} \times r_4, \ r_3 < C \\ 1, \ r_3 > C \end{cases} \quad (2)$$

$$\overline{W_2(i)} = \left(1 - e^{-|hng(i) - Shng|}\right) \times r_5 \times 2 \quad (3)$$

In Eqs. (2) and (3), r_3, r_4 and r_5 represent different random numbers within $[0, 1]$. The value of the $hng(t)$ is defined as follows:

$$hng(i) = \begin{cases} 0, \ Allfit(i) == BFit \\ hng(i) + H, \ Allfit(i) != BFit \end{cases} \quad (4)$$

where $Allfit(i)$ represents the fitness of each individual in current iteration. The following form is used to define the parameter of H (hunger sensation).

$$H = \begin{cases} LH \times (1 + r), \ TH < LH \\ TH, \ TH \geq LH \end{cases} \quad (5)$$

where $TH = ((F(i) - BFit)/(WF - BFit)) \times r_6 \times 2 \times (UB - LB)$. In here, WF denotes the worst fitness value obtained so far and LH is the lower bound. The feature space related upper and lower bounds are respec-

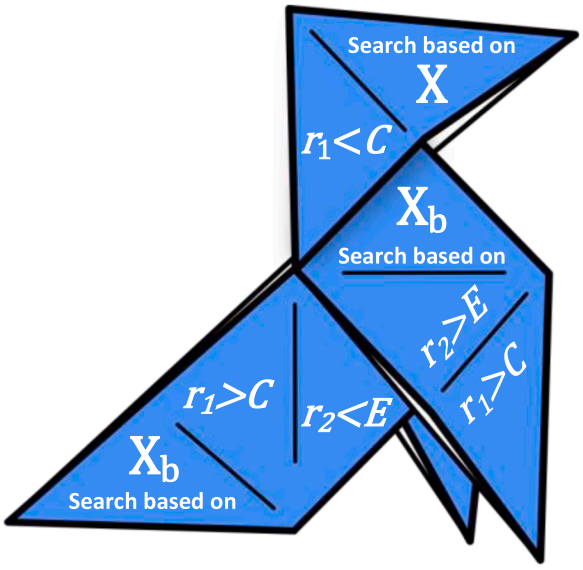


Fig. 1. Logic of HGS algorithm during optimization [19].

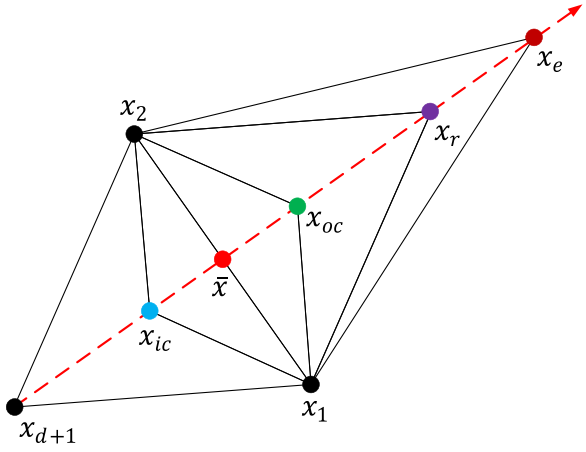


Fig. 2. Schematic diagram of NMS method.

tively represented by *UB* and *LB*. Fig. 1 provides a flowchart representing the logic of the HGS algorithm.

3. The proposed algorithm

3.1. Nelder-Mead simplex method

The Nelder-Mead simplex (NMS) method is a direct search mechanism that can provide an excellent intensification capability [20]. This method describes a d dimensional simplex having $d+1$ vertices (x_1, x_2, …x_d, x_{d+1}). A sequence of simplices is then generated iteratively in order to approximate an optimal point of an $f(x)$ objective function with the aim of reaching a relationship of $f(x_1) \leq f(x_2) \leq \ldots \leq f(x_{d+1})$. In the latter order, the best vertex is represented by x_1 and the worst one is x_{d+1}. To replace the worst vortex, the NMS method uses scalar coefficients of ρ, β, γ and δ (reflection, contraction, expansion and shrinkage). The reflection point is calculated as $x_r = \overline{x} + \rho(\overline{x} - x_{d+1})$ where $\overline{x}$ denotes the centroid point which is defined as follows.

$$\overline{x} = \frac{1}{d}\sum_{i=1}^{d} x_i \tag{6}$$

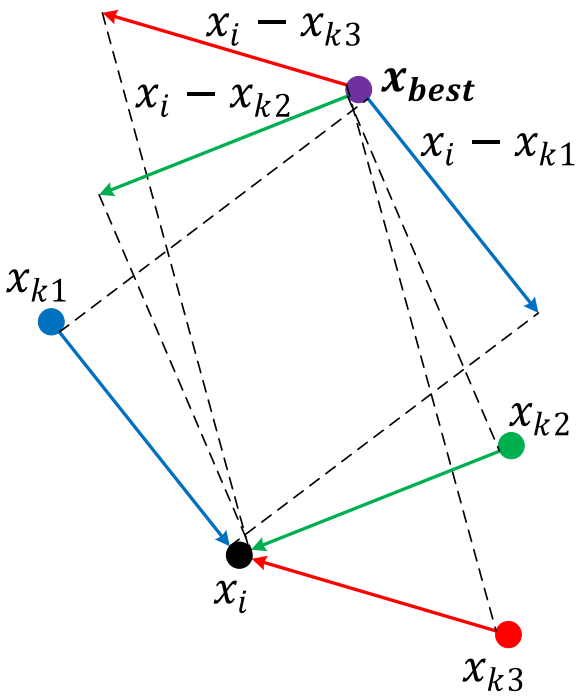


Fig. 3. Schematic diagram of RLM principle.

x_r replaces x_{d+1} if $f(x_1) \leq f(x_r) < f(x_d)$. In case of $f(x_r) < f(x_1)$, the expansion point is computed as $x_e = \overline{x} + \gamma(x_r - \overline{x})$. In the expansion stage of the NMS method, x_{d+1} is replaced by x_e for $f(x_e) < f(x_r)$, otherwise it is replaced by x_r. This is followed by computing the outside contraction point, for $f(x_d) \leq f(x_r) < f(x_{d+1})$, using $x_{oc} = \overline{x} + \beta(x_r - \overline{x})$. In this stage, x_{d+1} is replaced by x_{oc} for $f(x_{oc}) \leq f(x_r)$, otherwise, the last step of the NMS method (shrinkage) is performed. Meanwhile, an inside contraction point is computed for $f(x_{d+1}) \leq f(x_r)$ instead of the outside contraction point. The inside contraction point is computed as $x_{ic} = \overline{x} + \beta(x_{d+1} - \overline{x})$. In case of the inner contraction point, the x_{d+1} is replaced by x_{ic} for $f(x_{ic}) < f(x_{d+1})$ and the shrinkage step is performed otherwise. In the shrinkage step the definition of $v_i = x_1 + \delta(x_i - x_1)$ is used where $i = 2, 3, \ldots, d+1$. The latter definition helps constructing new points through shrinking them. The schematic diagram of the NMS method is provided in Fig. 2.

3.2. Random learning mechanism

The random learning mechanism (RLM) is a stochastic propagation model that has a good contribution towards increasing the diversification capability of the algorithms [21]. Therefore, it is feasible to avoid local optimum with the aid of the RLM. The RLM can mathematically be defined as follows.

$$x_{new} = \begin{cases} x_{best} + rand \times \left(x_i^t - x_{k1}^t\right); \ if \ f_{k1} < f_{k2} \ and \ f_{k1} < f_{k3} \\ x_{best} + rand \times \left(x_i^t - x_{k2}^t\right); \ if \ f_{k2} < f_{k1} \ and \ f_{k2} < f_{k3} \\ x_{best} + rand \times \left(x_i^t - x_{k3}^t\right); \ otherwise \end{cases} \tag{7}$$

In here, the optimal solution is denoted by x_{best}, a random number within $[0, 1]$ is shown by *rand* and the i^{th} individual in the population at t^{th} iteration is represented by x_i^t. Randomly chosen three different individuals are represented by x_{k1}^t, x_{k2}^t and x_{k3}^t whereas their fitness values are respectively shown by f_{k1}, f_{k2} and f_{k3}. The schematic diagram of the RLM is given in Fig. 3.

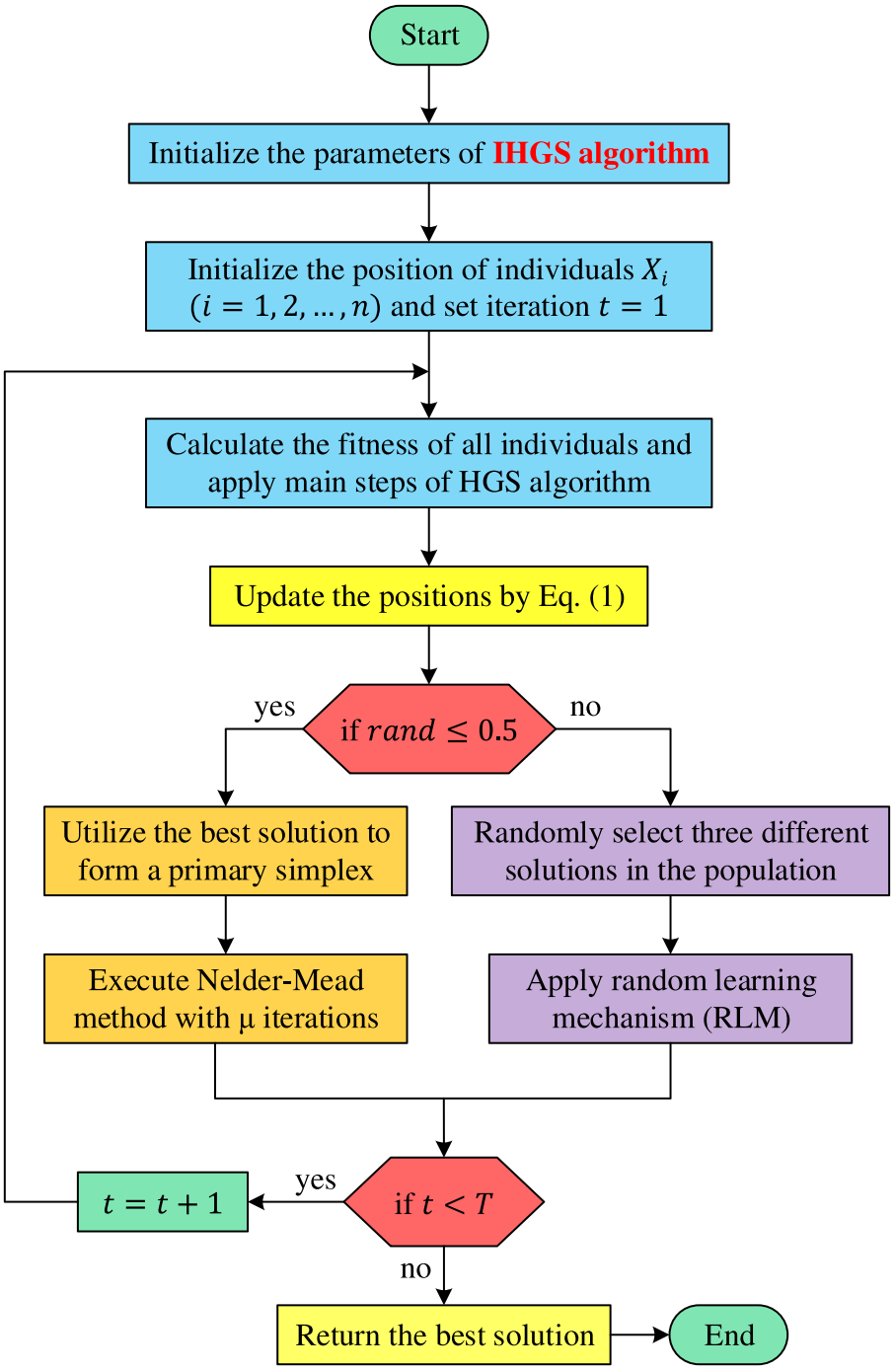


Fig. 4. Flowchart of proposed IHGS algorithm.

3.3. The proposed IHGS algorithm

The proposed IHGS algorithm employs NMS method to reach an increased intensification and RLM technique for improved diversification. As depicted in Fig. 4, the proposed IHGS algorithm starts by initialization of parameters and the individual positions. Then the fitness of all individuals is calculated and the original version of the HGS algorithm is performed in order to update the positions of the individuals. After this step, a random number (*rand*) is compared with a pre-defined constant value of 0.5. In case of smaller or equal random values than the pre-defined constant value, a simplex is formed from the best solution and the NMS method is performed for μ $(d+1)$ iterations. If the generated random value is bigger than the pre-defined constant value, then three different solutions are selected from the population randomly and the RLM is performed. This process takes place until the termination condition (maximum number of iterations) is met. In this way, the IHGS algorithm reaches an excellent balance between intensification and diversification stages.

4. Experimental results on various benchmark functions

4.1. Details of used benchmark functions

To demonstrate the excellent capability of the proposed IHGS algorithm has initially been tested agains the unimodal, multimodal, fixed-dimensional and CEC2019 benchmark functions. The details (name,

Table 1
Employed unimodal benchmark functions.

ID	Name	Dimension	Search range	F_{min}
F1	Sphere	30	$[-100, 100]$	0
F2	Schwefel 2.2	30	$[-10, 10]$	0
F3	Schwefel 1.2	30	$[-100, 100]$	0
F4	Schwefel 2.21	30	$[-100, 100]$	0
F5	Rosenbrock	30	$[-30, 30]$	0
F6	Step	30	$[-100, 100]$	0
F7	Quartic	30	$[-1.28, 1.28]$	0

Table 2
Employed multimodal benchmark functions.

ID	Name	Dimension	Search range	F_{min}
F8	Schwefel	30	$[-500, 500]$	−1.2569E+04
F9	Rastrigin	30	$[-5.12, 5.12]$	0
F10	Ackley	30	$[-32, 32]$	0
F11	Griewank	30	$[-600, 600]$	0
F12	Penalized	30	$[-50, 50]$	0
F13	Penalized2	30	$[-50, 50]$	0

Table 3
Employed fixed-dimensional benchmark functions.

ID	Name	Dimension	Search range	F_{min}
F14	Foxholes	2	$[-65.536, 65.536]$	0.998
F15	Kowalik	4	$[-5, 5]$	3.0749E−04
F16	Six- Hump Camel	2	$[-5, 5]$	−1.0316
F17	Branin	2	$[-5, 10] \times [0, 15]$	0.39789
F18	Goldstein-Price	2	$[-2, 2]$	3
F19	Hartman 3	3	$[0, 1]$	−3.8628
F20	Hartman 6	6	$[0, 1]$	−3.322
F21	Shekel 5	4	$[0, 10]$	−10.1532
F22	Shekel 7	4	$[0, 10]$	−10.4029
F23	Shekel 10	4	$[0, 10]$	−10.5364

Table 4
Employed CEC2019 benchmark functions.

ID	Name	Dimension	Search range	F_{min}
F24	Storn's Chebyshev Polynomial Fitting Problem	9	$[-8192, 8192]$	1
F25	Inverse Hilbert Matrix Problem	16	$[-16,384, 16, 384]$	1
F26	Lennard-Jones Minimum Energy Cluster	18	$[-4, 4]$	1
F27	Rastrigin's Function	10	$[-100, 100]$	1
F28	Griewangk's Function	10	$[-100, 100]$	1
F29	Weierstrass Function	10	$[-100, 100]$	1
F30	Modified Schwefel's Function	10	$[-100, 100]$	1
F31	Expanded Schaffer's F6 Function	10	$[-100, 100]$	1
F32	Happy Cat Function	10	$[-100, 100]$	1
F33	Ackley Function	10	$[-100, 100]$	1

dimension, range and global minimum) of those benchmark functions are respectively listed in Tables 1–4. It is feasible to demonstrate the performance of the proposed algorithm in terms of diversification, intensification and solution quality using those test suites. For each benchmark function, the algorithms were run for 30 times using a population size of 30 and a maximum iteration number of 500. The parameters of C and LH for both original and the improved versions of HGS algorithms were set to 0.03 and 100, respectively. The additional NM parameters (embedded in IHGS algorithm) of ρ, γ, β and δ were set to 1, 2, 0.5 and 0.5, respectively.

4.2. Intensification and diversification capabilities

The performance of the proposed IHGS algorithm was initially tested for its intensification and diversification capability. In this regard, the benchmark functions with unimodal nature, listed in Table 1, can be used to examine the intensification capability whereas the ones with the multimodal, listed in Table 2, can be employed for the diversification capability. On the other hand, the fixed-dimensional benchmark functions listed in Table 3 are good for evaluation of the solution quality of the algorithm. Tables 5–7 respectively provide the comparative statistical results (mean, standard deviation, best and worst) obtained from the unimodal, multimodal, and low-dimensional test functions. In terms of comparisons, the performance of the proposed IHGS algorithm was tested against the original version of the HGS algorithm as the latter one has already been demonstrated to perform better than other state-of-the-art and well performing algorithms. As demonstrated from the numerical values of the related tables, the proposed IHGS algorithm performs more excellently compared to original form of the HGS algorithm.

4.3. Results comparisons using CEC2019 benchmark functions

To further demonstrate the excellent performance of the proposed IHGS algorithm, the challenging benchmark functions from CEC2019 test suite was also used. The obtained results from CEC2019 test suite are comparatively provided in Table 8. As demonstrated in the respective numerical results the proposed IHGS has an overall superiority since it achieves either the best mean value for most of the test functions and similar optimal values for the remaining few ones.

5. Detailed model of buck converter system

The buck converter is a nonlinear system that is used to convert a higher level of DC voltage to a lower level. The conversion is facilitated via pulse width modulation technique (switching on/off a transistor at high frequency). As shown in Fig. 5, the buck converter is a nonlinear system consisting of a DC voltage source, switching device (a MOSFET or IGBT), diode, filter capacitor and inductor and the load. The variation of the voltage is controlled with the on time of the switching.

As can be observed from Fig. 5, the buck converter is a DC–DC switching circuit making it a time-varying and nonlinear system. Therefore, the respective system needs to be linearized in order to be able to design an appropriate linear controller. In this regard, state-space averaging or circuit averaging methods may be employed [24]. However, in this study, a method known as switching signal-flow graph [25] was be employed to derive the small-signal model of the buck system. The latter method is an extension of the signal-flow graph theory [25] and also based on the state-space-averaging method. Therefore, the obtained transfer functions with this method are similar to that of obtained by the state-space-averaging method. However, the employed model is a visualized method helping to quickly obtain the transfer functions of the system. The small-signal model of buck converter system is demonstrated in Fig. 6.

It is worth noting that the details regarding the derivation of the respective model is not provided in here in order not to distract the readers. For details on the derivation, the readers are referred to ref. [25]. Considering the latter discussion, the transfer functions provided in Eqs. (8), (9), (10) and (11) can be obtained for the buck converter system by using the respective signal-flow graph, graph algebra and Mason gain formula [26].

$$G_{vd}(s) = \frac{\Delta V_o(s)}{\Delta D(s)} = V_g \cdot \frac{\frac{1}{LC}}{s^2 + \frac{s}{RC} + \frac{1}{LC}} \tag{8}$$

$$G_{vg}(s) = \frac{\Delta V_o(s)}{\Delta V_g(s)} = D \cdot \frac{\frac{1}{LC}}{s^2 + \frac{s}{RC} + \frac{1}{LC}} \tag{9}$$

Table 5
Comparative statistical results for unimodal benchmark functions.

ID	Algorithm	Mean	Standard Deviation	Best	Worst
F1	HGS	9.2045E−160	4.7854E−159	0	2.6244E−158
	IHGS	0	0	0	0
F2	HGS	2.0745E−83	9.6959E−83	0	5.2667E−82
	IHGS	0	0	0	0
F3	HGS	1.5183E−55	8.3163E−55	0	4.5550E−54
	IHGS	0	0	0	0
F4	HGS	4.2263E−62	2.3149E−61	0	1.2679E−60
	IHGS	0	0	0	0
F5	HGS	1.2620E+01	1.2826E+01	1.1624E−05	2.5606E+01
	IHGS	0	0	0	0
F6	HGS	5.8382E−06	8.9703E−06	2.4287E−08	3.4663E−05
	IHGS	0	0	0	0
F7	HGS	6.8375E−04	7.1945E−04	1.5868E−06	2.3306E−03
	IHGS	8.5579E−06	1.0485E−05	8.6407E−07	5.0378E−05

Table 6
Comparative statistical results for multimodal benchmark functions.

ID	Algorithm	Mean	Standard Deviation	Best	Worst
F8	HGS	−1.2448E+04	6.4825E+02	−1.2569E+04	−9.0162E+03
	IHGS	−1.2569E+04	0	−1.2569E+04	−1.2569E+04
F9	HGS	0	0	0	0
	IHGS	0	0	0	0
F10	HGS	8.8818E−16	0	8.8818E−16	8.8818E−16
	IHGS	8.8818E−16	0	8.8818E−16	8.8818E−16
F11	HGS	0	0	0	0
	IHGS	0	0	0	0
F12	HGS	1.0759E−07	7.7998E−08	4.7778E−09	3.0107E−07
	IHGS	1.5705E−32	0	1.5705E−32	1.5705E−32
F13	HGS	2.5298E−02	9.6784E−02	1.5809E−08	4.1746E−01
	IHGS	1.3498E−32	0	1.3498E−32	1.3498E−32

Table 7
Comparative statistical results for fixed-dimensional benchmark functions.

ID	Algorithm	Mean	Standard Deviation	Best	Worst
F14	HGS	3.6020E+00	4.3921E+00	9.9800E−01	1.0763E+01
	IHGS	9.9800E−01	0	9.9800E−01	9.9800E−01
F15	HGS	6.9403E−04	3.0437E−04	3.0757E−04	1.5941E−03
	IHGS	3.0749E−04	0	3.0749E−04	3.0749E−04
F16	HGS	−1.0316E+00	0	−1.0316E+00	−1.0316E+00
	IHGS	−1.0316E+00	0	−1.0316E+00	−1.0316E+00
F17	HGS	3.9789E−01	0	3.9789E−01	3.9789E−01
	IHGS	3.9789E−01	0	3.9789E−01	3.9789E−01
F18	HGS	3.0000E+00	0	3.0000E+00	3.0000E+00
	IHGS	3.0000E+00	0	3.0000E+00	3.0000E+00
F19	HGS	−3.8628E+00	0	−3.8628E+00	−3.8628E+00
	IHGS	−3.8628E+00	0	−3.8628E+00	−3.8628E+00
F20	HGS	−3.2798E+00	6.7812E−02	−3.3220E+00	−3.1376E+00
	IHGS	−3.3220E+00	0	−3.3220E+00	−3.3220E+00
F21	HGS	−9.3342E+00	2.2269E+00	−1.0153E+01	−8.8098E−01
	IHGS	−1.0153E+01	0	−1.0153E+01	−1.0153E+01
F22	HGS	−1.0049E+01	1.3485E+00	−1.0403E+01	−5.0877E+00
	IHGS	−1.0403E+01	0	−1.0403E+01	−1.0403E+01
F23	HGS	−9.6347E+00	2.0497E+00	−1.0536E+01	−5.1285E+00
	IHGS	−1.0536E+01	0	−1.0536E+01	−1.0536E+01

$$G_{id}(s) = \frac{\Delta I_L(s)}{\Delta D(s)} = V_g.\frac{\frac{1}{L}.\left(s+\frac{1}{RC}\right)}{s^2+\frac{s}{RC}+\frac{1}{LC}} \tag{10}$$

$$G_{ig}(s) = \frac{\Delta I_L(s)}{\Delta V_g(s)} = D.\frac{\frac{1}{L}.\left(s+\frac{1}{RC}\right)}{s^2+\frac{s}{RC}+\frac{1}{LC}} \tag{11}$$

As this work aims to observe the effect of the duty cycle on the output voltage, the definition provided in Eq. (8) was considered in this paper. In this regard, the source voltage, V_g, operating point voltage, V_{ref}, load resistance, R, filter inductor, L, filter capacitor, C, duty cycle, D, and the switching frequency, f_s, were respectively chosen to be 36 V, 12 V, 6 Ω, 1 mH, 100 μF, 1/3 and 40 kHz such that the open-loop step response of the buck converter corresponding to a step change of $\delta d = 1/36$ can be obtained in duty cycle ratio.

In Fig 7, the pole-zero map (a) and the step response of the buck converter system is provided. As shown in the respective figure, the open-loop step response of the buck converter is oscillatory with high overshoot and settling time. Therefore, a controller must be employed to overcome the related issue so that the transient response of the buck converter system can be enhanced, and its output voltage can be regulated. To address the latter requirement, a FOPID controller was employed in this work due to its robustness to uncertainties and load

Table 8
Comparative statistical results for CEC2019 benchmark functions.

ID	Algorithm	Mean	SD	Best	Worst
F24	HGS	4.4521E+04	7.1020E+03	3.8529E+04	7.3728E+04
	IHGS	4.0571E+04	1.7671E+03	3.8128E+04	4.3557E+04
F25	HGS	1.7343E+01	1.6850E−13	1.7343E+01	1.7343E+01
	IHGS	1.7343E+01	3.7449E−15	1.7343E+01	1.7343E+01
F26	HGS	1.2702E+01	0	1.2702E+01	1.2702E+01
	IHGS	1.2702E+01	0	1.2702E+01	1.2702E+01
F27	HGS	4.2892E+01	2.0516E+01	9.9536E+00	8.7571E+01
	IHGS	4.0199E+01	2.0362E+01	9.9496E+00	6.0694E+01
F28	HGS	1.2509E+00	1.7235E−01	1.0394E+00	1.7523E+00
	IHGS	1.1674E+00	1.4148E−01	1.0099E+00	1.4925E+00
F29	HGS	4.2834E+00	1.1379E+00	2.7374E+00	7.0811E+00
	IHGS	3.4577E+00	1.0881E+00	1.8572E+00	5.2139E+00
F30	HGS	1.8715E+02	2.0085E+02	−2.6499E+02	6.6012E+02
	IHGS	1.2853E+02	2.4569E+02	−2.7756E+02	5.0897E+02
F31	HGS	5.3285E+00	5.6196E−01	4.1936E+00	6.0311E+00
	IHGS	5.0973E+00	9.2372E−01	3.1997E+00	5.9815E+00
F32	HGS	2.9541E+00	2.9079E−01	2.4362E+00	3.4586E+00
	IHGS	2.5811E+00	1.6095E−01	2.3966E+00	2.9076E+00
F33	HGS	2.0021E+01	3.6123E−02	1.9999E+01	2.0162E+01
	IHGS	2.0013E+01	2.0940E−02	1.9997E+01	2.0057E+01

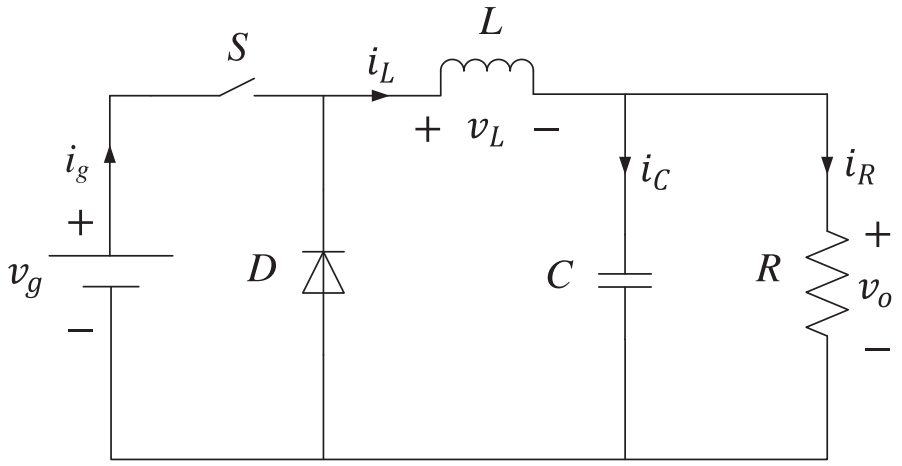


Fig. 5. Buck converter system.

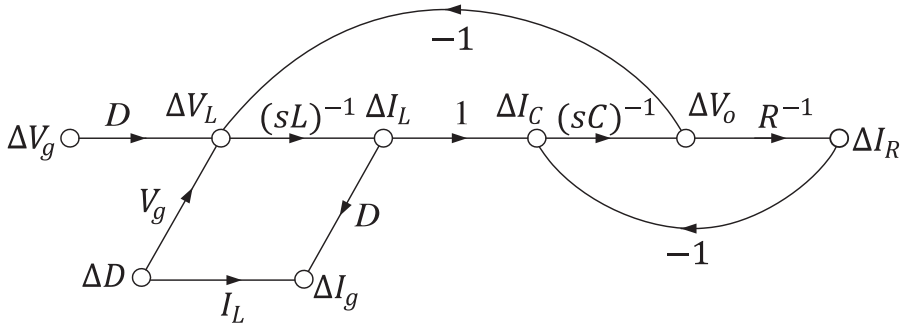


Fig. 6. Small-signal model of buck converter system.

disturbances for dynamic systems [27].

6. FOPID controller for buck converter system

6.1. A review of fractional calculus

It is feasible to encounter several different approaches that have been proposed for fractional calculus [28]. Caputo, Riemann-Liouville and Grunwald-Letnikov are only a few and most widely used definitions for fractional-order calculus [13]. The β^{th} order derivative of an f function within the limits of $[a,\ t]$ can be defined with the Grunwald-Letnikov's approach as follows:

$$D^{\beta} = \lim_{h\to 0} \frac{1}{h^{\beta}} \sum_{r=0}^{\left[\frac{t-a}{h}\right]} (-1)^{r} \binom{n}{r} f(t-rh) \tag{12}$$

where n is an integer that must satisfy $n-1 < \beta < n$ and h is the time

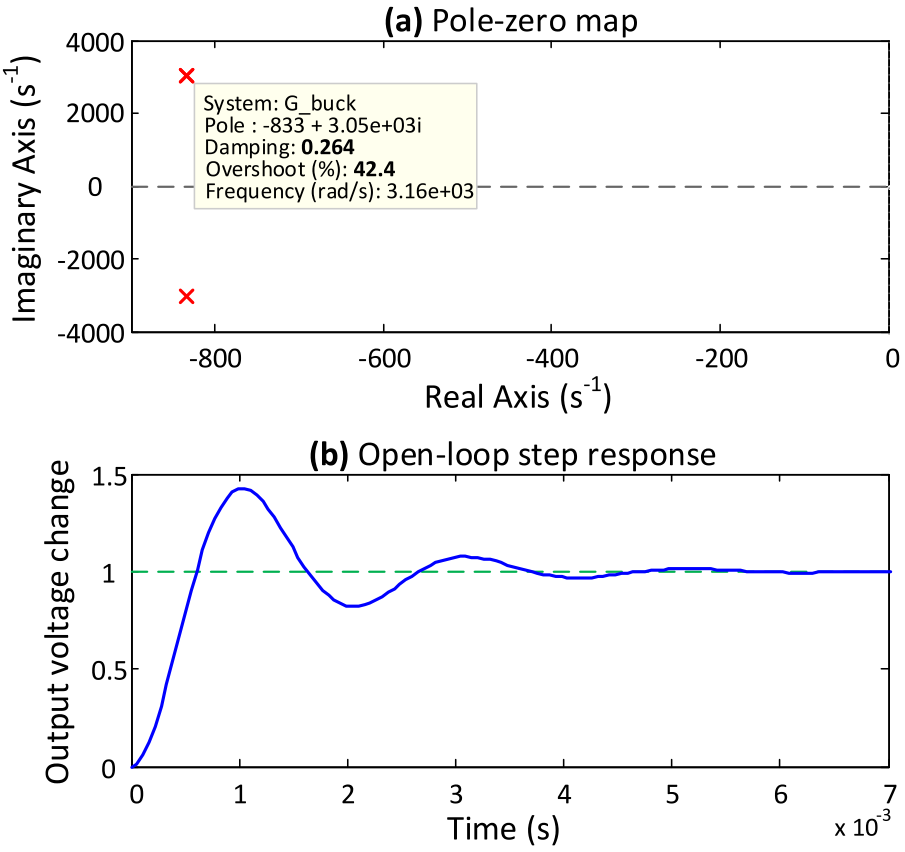


Fig. 7. Pole-zero map (a) and step response (b) of the system.

step. The binomial coefficient is defined as in Eq. (13).

$$\binom{n}{r} = \frac{\Gamma(n+1)}{\Gamma(r+1)\Gamma(n-r+1)} \tag{13}$$

The Gamma function can be described as follows.

$$\Gamma(x) = \int_0^\infty t^{x-1} e^{-t} dt \tag{14}$$

The definition of Grunwald-Letnikov is favorable in terms of obtaining numerical solution of differential equations [29]. Riemann and Liouville proposed another definition that uses integer-order derivative and integral as described in Eq. (15) in order to avoid the disadvantage of using the limit and the sum in the definition of Grunwald-Letnikov.

$$D^\beta = D^n J^{n-\beta} f(t) = \frac{1}{\Gamma(n-\beta)} \left(\frac{d}{dt}\right)^n \int_a^t \frac{f(\tau)}{(t-\tau)^{\beta-n+1}} d\tau \tag{15}$$

In here, J represents the integral operator, n is an integer that must satisfy $n-1 < \beta < n$ and β is a real number. The Riemann-Liouville definition is appropriate to find the analytical solution for simple functions such as e^t and $\cos(t)$ [13]. In terms of engineering applications, on the other hand, the Caputo definition is most popular [30] as it operates based on the connection between the types of the initial conditions and the fractional derivative. The latter approach is defined as given in Eq. (16).

$$D^\beta = \frac{1}{\Gamma(n-\beta)} \int_a^t \frac{f^n(\tau)}{(t-\tau)^{\beta-n+1}} d\tau \tag{16}$$

6.2. Digital implementation

A significant issue regarding the aforementioned definitions is that they suffer from applicability in terms of real-time implementation [31]. To overcome this issue, Oustaloup proposed an approximation method that uses recursive pole-zero distributions [32]. The Oustaloup's approximation method is widely employed in literature in terms of tuning FOPID controller [17,33–35]. Besides, the Oustalop's method can be observed to dominate over other definitions in case of practical implementations of the fractional-order calculus [28]. Due to above mentioned reasons, Oustaloup's recursive approximation method has also been employed for this study. In the Oustaloup's method, the β^{th} order derivative (s^β) is approximated as given in Eq. (17).

$$s^\beta \approx \omega_h^\beta \cdot \prod_{k=-N}^{N} \frac{s+\omega_k'}{s+\omega_k} \tag{17}$$

The poles and the zeros of the latter equation is defined as given in Eqs. (18) and (19), respectively.

$$\omega_k = \omega_b \left(\frac{\omega_h}{\omega_b}\right)^{\frac{k+N+(1+\beta)/2}{2N+1}} \tag{18}$$

$$\omega_k' = \omega_b \left(\frac{\omega_h}{\omega_b}\right)^{\frac{k+N+(1-\beta)/2}{2N+1}} \tag{19}$$

In the latter definitions, $2N+1$ represents the order whereas (ω_b, ω_h) stands for the frequency range of the approximation filter, respectively. In this work, 11^{th} order ($N = 5$) Oustaloup's recursive approximation has been considered within the frequency band of $\omega \in (10^{-3}, 10^3)$ rad/s which is the most typical range for FOPID applications [8].

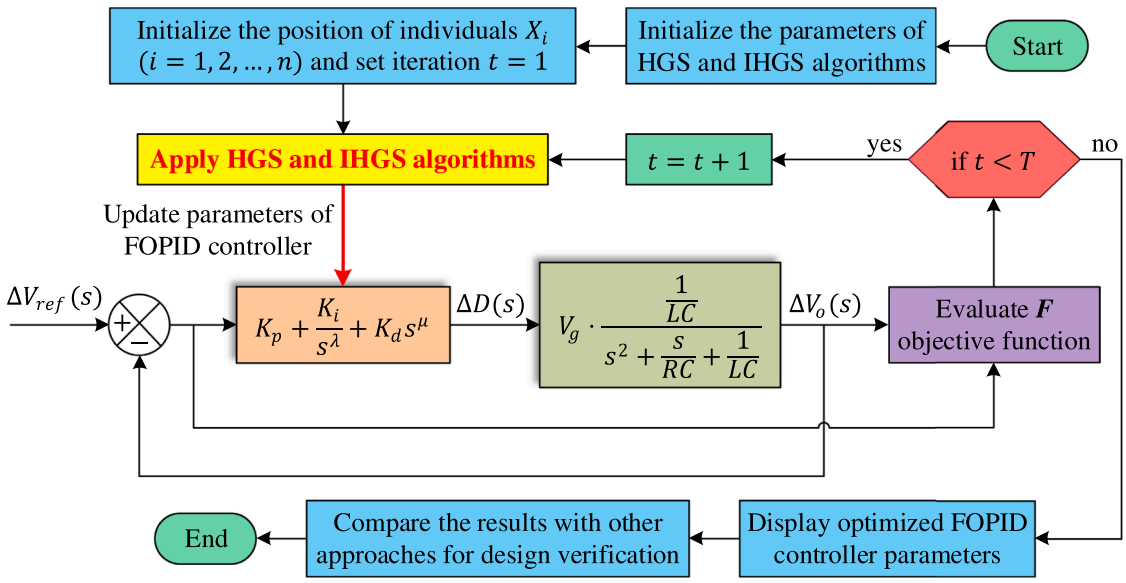


Fig. 8. Implementation stage of the HGS and the proposed IHGS algorithms.

6.3. FOPID controlled buck converter system

The following equation represents the transfer function of a FOPID ($PI^\lambda D^\mu$) controller:

$$G_{FOPID}(s) = K_p + \frac{K_i}{s^\lambda} + K_d s^\mu \tag{20}$$

where K_p, K_i, K_d are proportional, integral, and derivative gains whereas λ and μ are fractional integral, and fractional derivative orders, respectively. The latter two fractional terms are adjustable within $(0,\ 2)$. Form this point of view, the FOPID controller provides an extra two degrees of freedom compared to conventional PID controller. Meanwhile, a FOPID controller can be reduced to a conventional PID controller if the fractional orders of λ and μ are set to 1. The closed-loop transfer function of buck converter system with FOPID controller is provided in the following form:

$$T_{closed-loop}(s) = \frac{\Delta V_o(s)}{\Delta V_{ref}(s)} = \frac{G_{vd}(s)G_{FOPID}(s)}{1 + G_{vd}(s)G_{FOPID}(s)} \tag{21}$$

where $\Delta V_o(s)$ and $\Delta V_{ref}(s)$ are the changes in output and reference voltages, respectively. The following closed-loop transfer function can be obtained for the buck converter system by substituting the Eqs. (8) and (20) into Eq. (21).

$$T_{closed-loop}(s) = \frac{\Delta V_o(s)}{\Delta V_{ref}(s)} = \frac{\left(V_g \cdot \frac{\frac{1}{LC}}{s^2 + \frac{s}{RC} + \frac{1}{LC}}\right)\left(K_p + \frac{K_i}{s^\lambda} + K_d s^\mu\right)}{1 + \left(V_g \cdot \frac{\frac{1}{LC}}{s^2 + \frac{s}{RC} + \frac{1}{LC}}\right)\left(K_p + \frac{K_i}{s^\lambda} + K_d s^\mu\right)} \tag{22}$$

7. A novel approach for FOPID controller design of buck converter system

7.1. Objective function and related parameters

To enhance the output voltage regulation of the buck converter, the integral of squared error (ISE) performance index can be employed as an objective. The related performance index is given with the following form:

$$ISE = \int_0^\infty e^2(t) \cdot dt \tag{23}$$

where $e(t)$ represents the error between the reference $\delta v_{ref}(t)$ and the output $\delta v_o(t)$ voltages, thus, $e(t) = \delta v_{ref}(t) - \delta v_o(t)$. Although the ISE objective function is good for minimizing the overshoots, it lacks providing desired settling times. Considering this fact, the following novel objective function (F) was also proposed in this study.

$$F = \phi \cdot ISE + (1 - \phi) \cdot T_s \tag{24}$$

In the F objective function, ϕ stands for a balancing coefficient between ISE performance index and the settling time (T_s) which has a range of $(0,\ 1)$. After extensive simulations, the value for the related coefficient was found to be 0.6 in order to reach optimal performance in this study. Apart from this novel objective function, the following limits for the FOPID controller and the designated values for the parameters of the algorithms were also employed to achieve an efficient operation of the system.

Limits for the FOPID controller: $1 \leq K_p \leq 50$; $0.01 \leq K_i \leq 10$; $0.001 \leq K_d \leq 0.02$; $0 < \lambda < 2$ and $0 < \mu < 2$.

HGS and IHGS algorithms related parameters: Number of runs = 30; dimension (variable number) size = 5; population size = 50; total iteration number = 40; $C = 0.03$, $LH = 100$, $\rho = 1$, $\gamma = 2$, $\beta = 0.5$, $\delta = 0.5$ (the last four parameters are the NMS related parameters embedded in IHGS algorithm).

7.2. Implementation stage

The detailed implementation stage of the HGS and the proposed IHGS algorithms is provided in Fig. 8. As can be observed, the related algorithms are initialized and then performed to tune the FOPID controller parameters with the aid of the novel F objective function. For the minimization of the F objective function, the error between the reference voltage, $\Delta V_{ref}(s)$ and the output voltage, $\Delta V_o(s)$, is considered. In this way, the FOPID controller parameters are adjusted optimally, and the efficient operation of the buck converter system is achieved.

After the implementation procedure given in Fig. 8, the proposed IHGS algorithm obtained the best FOPID controller parameters as $K_p = 37.6492$; $K_i = 5.4315$; $K_d = 0.01758$; $\lambda = 1.0167$ and $\mu = 1.0285$. Substituting the latter obtained values for the FOPID controller and the buck converter system values listed in Section 5 into Eq. (22), the transfer function given in Eq. (25) can be obtained for the proposed IHGS algorithm based FOPID controlled buck converter system.

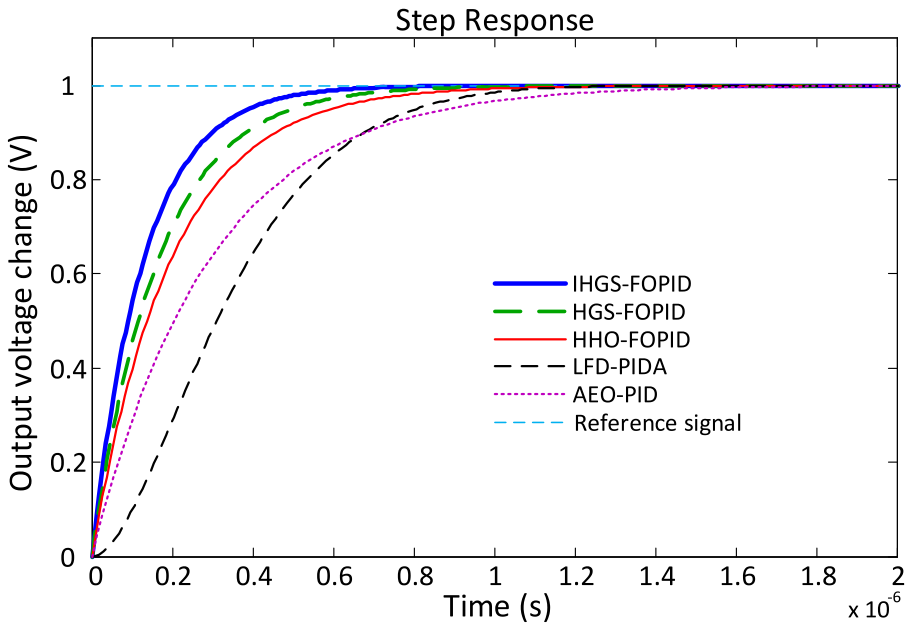


Fig. 9. Step responses of buck converter system for various approaches.

Table 9
Numerical transient response performance of different methods.

Controller type	Overshoot (%)	Rise time (s)	Settling time (s)	Peak time (s)
IHGS-FOPID	0	2.8510E−07	5.0765E−07	1.3686E−06
HGS-FOPID	0	3.6454E−07	6.4930E−07	1.7496E−06
HHO-FOPID [18]	0	4.3528E−07	7.7523E−07	2.0892E−06
LFD-PIDA [7]	0.0124	5.7605E−07	9.5433E−07	1.5356E−06
AEO-PID [6]	0	6.4613E−07	1.1454E−06	2.0223E−06

$$TF_{IHGS-FOPID}(s) = \frac{0.63288s^{2.0452} + 1355.4s^{1.0167} + 195.53}{10^{-7}s^{3.0167} + 0.63288s^{2.0452} + 0.00016667s^{2.0167} + 1356.4s^{1.0167} + 195.53} \quad (25)$$

Similarly, the best FOPID controller parameters for the original version of the HGS algorithm were found as $K_p = 25.1434$; $K_i = 6.2831$; $K_d = 0.01196$; $\lambda = 1.1312$ and $\mu = 1.0487$. Substituting the latter obtained values for the FOPID controller and the buck converter system values listed in Section 5 into Eq. (22), the transfer function given in Eq. (26) can be obtained for the original version of HGS algorithm based FOPID controlled buck converter system.

$$TF_{HGS-FOPID}(s) = \frac{0.43056s^{2.1799} + 905.16s^{1.1312} + 226.19}{10^{-7}s^{3.1312} + 0.43056s^{2.1799} + 0.00016667s^{2.1312} + 906.16s^{1.1312} + 226.19} \quad (26)$$

8. Comparative simulation results and discussions

8.1. Selected approaches

In order to perform extensive simulations comparatively, the best performing methods of Harris hawks optimization algorithm based FOPID (HHO-FOPID) controller [18], Lévy flight distribution algorithm based PIDA (LFD-PIDA) controller [7] and artificial ecosystem optimization algorithm based PID (AEO-PID) controller [6] were used in this study. As can also be observed from those methods, each of them uses different algorithms and controller types making them convenient to assess the performance of the HGS based FOPID (HGS-FOPID) and the proposed IHGS based FOPID (IHGS-FOPID) controllers employed for the buck converter system.

8.2. Transient response

The comparative transient response of the buck converter system for the approaches of HHO-FOPID [18], LFD-PIDA [7] and AEO-PID [6] along with HGS-FOPID and IHGS-FOPID controllers is provided in Fig. 9 by considering a reference voltage change of 1 V ($\delta v_{ref}(t) = 1\ V$).

In addition, the overshoot, rise time, settling time and peak time related performance of those methods are also provided in Table 9 numerically. As can be observed from the related figure and the table, apart from the LFD-PIDA, all algorithms reached the no overshoot. However, the proposed IHGS-FOPID method has reached the lowest values for the rise, settling and peak times confirming its more excellent capability in terms of transient response of the buck converter system.

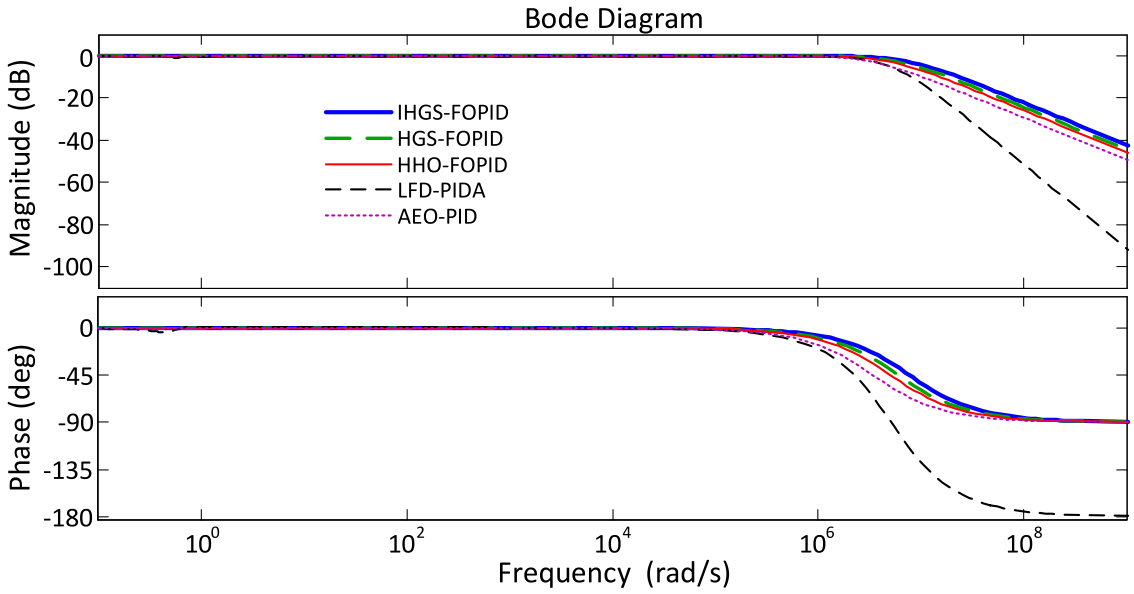


Fig. 10. Bode plots of buck converter system for various approaches.

8.3. Frequency response

The comparative Bode plot of the buck converter system for the approaches of HHO-FOPID [18], LFD-PIDA [7] and AEO-PID [6] along with HGS-FOPID and IHGS-FOPID controllers is provided in Fig. 10. In addition, the gain margin, phase margin and bandwidth related performance of those methods are provided in Table 10 numerically. It can be seen from those results that all the methods have similar performance in terms of gain margin, the proposed IHGS-FOPID method provided the highest bandwidth and the second highest phase margin compared to other methods showing the good performance of the proposed method in terms of frequency response of the buck converter system.

Table 10
Numerical frequency response performance of different methods.

Controller type	Gain margin (dB)	Phase margin (deg)	Bandwidth (Hz)
IHGS-FOPID	Inf.	179.9994	7.6876E+06
HGS-FOPID	Inf.	179.9874	6.0129E+06
HHO-FOPID [18]	Inf.	179.9989	5.0356E+06
LFD-PIDA [7]	Inf.	180	3.7326E+06
AEO-PID [6]	Inf.	178.1149	3.3886E+06

8.4. Robustness performance

The robustness of a control method holds a crucial importance in terms of maintaining the stability of a system for unexpected conditions. In this study several different cases such as parameter uncertainty, load voltage fluctuation, input voltage fluctuation and the measurement noise were considered to assess the robustness of the proposed method comparatively.

8.4.1. Parameter uncertainty

In terms of the performance of the proposed IHGS-FOPID controller for parameter uncertainties of the buck converter system, the parameters of L and C were separately increased and decreased within $\pm 20\%$ and $\pm 25\%$, respectively. Table 11 provides the comparative obtained simulation results for different control methods. As seen from the latter table, apart from a negligible overshoot for the case of 25% increase in C parameter, the proposed IHGS-FOPID controller performs better for all performance metrics of different cases confirming the more excellent

Table 11
The robustness of different control methods for parameter uncertainties of the buck converter system.

Case	Controller type	Overshoot (%)	Rise time (s)	Settling time (s)	Peak time (s)
20% decrease in L parameter	IHGS-FOPID	0	2.2808E−07	4.0611E−07	1.0948E−06
	HGS-FOPID	0	2.9163E−07	5.1940E−07	1.3997E−06
	HHO-FOPID [18]	0	3.4822E−07	6.2015E−07	1.6713E−06
	LFD-PIDA [7]	1.0376	4.4278E−07	6.8321E−07	9.5249E−07
	AEO-PID [6]	0.0400	5.1707E−07	9.1740E−07	2.4863E−06
20% increase in L parameter	IHGS-FOPID	0	3.4212E−07	6.0915E−07	1.6423E−06
	HGS-FOPID	0	4.3746E−07	7.7922E−07	2.0995E−06
	HHO-FOPID [18]	0	5.2234E−07	9.3032E−07	2.5070E−06
	LFD-PIDA [7]	0	7.2094E−07	1.2615E−06	2.8253E−06
	AEO-PID [6]	0	7.7511E−07	1.3727E−06	2.4271E−06
25% decrease in C parameter	IHGS-FOPID	0	2.1386E−07	3.8097E−07	1.0264E−06
	HGS-FOPID	0	2.7346E−07	4.8732E−07	1.3121E−06
	HHO-FOPID [18]	0	3.2654E−07	5.8194E−07	1.5668E−06
	LFD-PIDA [7]	1.5619	4.1190E−07	6.2592E−07	8.7469E−07
	AEO-PID [6]	0.0251	4.8497E−07	8.6152E−07	2.3305E−06
25% increase in C parameter	IHGS-FOPID	0.0036	3.5632E−07	6.3413E−07	1.7108E−06
	HGS-FOPID	0	4.5559E−07	8.1108E−07	2.1871E−06
	HHO-FOPID [18]	0.0022	5.4397E−07	9.6820E−07	2.6117E−06
	LFD-PIDA [7]	0	7.5810E−07	1.3370E−06	3.0045E−06
	AEO-PID [6]	0	8.0705E−07	1.4275E−06	2.5286E−06

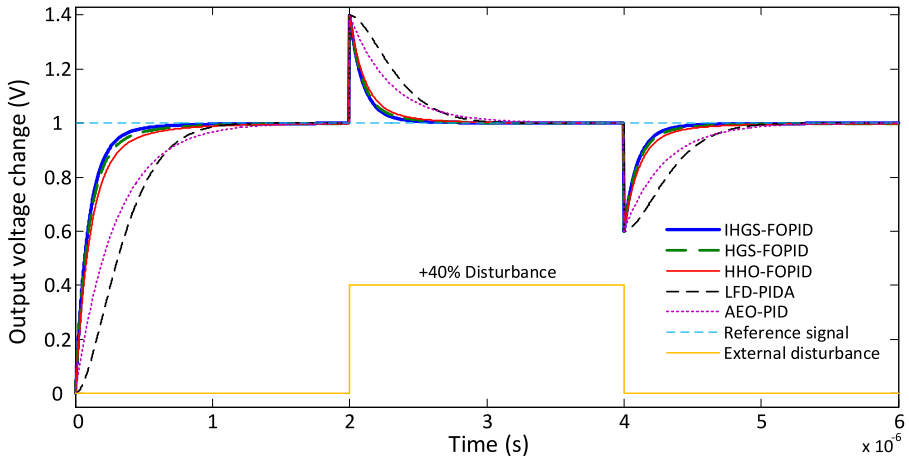


Fig. 11. Comparative performance of different methods against load voltage fluctuation.

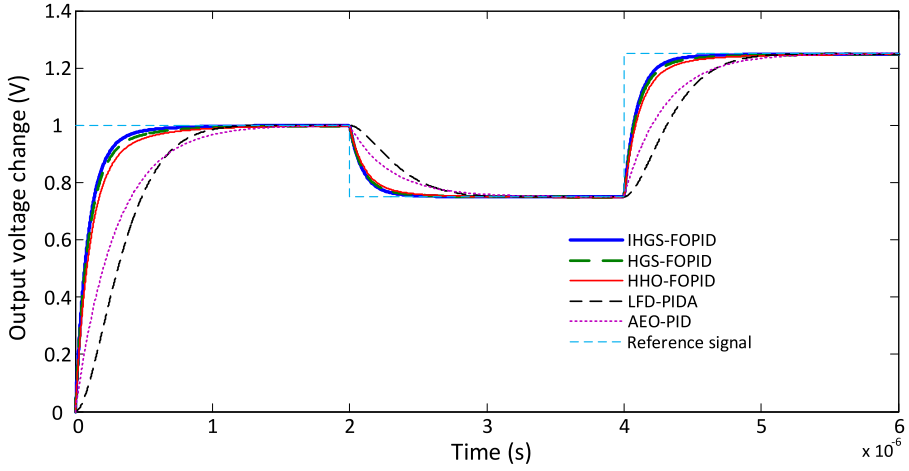


Fig. 12. Comparative performance of different methods against input voltage fluctuation.

robustness of the proposed method to the parameter uncertainties.

8.4.2. *Load voltage fluctuation*

The performance of the proposed IHGS-FOPID controller approach for the buck converter system for suppression of unexpected disturbances were also analyzed. In this regard, a 40% disturbance was introduced into output voltage at $t = 2$ *s* and removed at $t = 4$ *s*. Fig. 11 illustrates the comparative responses of different methods during such a disturbance. As can be observed from the respective figure, all methods were able to suppress the introduced unexpected disturbance, however, the proposed IHGS-FOPID controller was able to suppress the related disturbance faster and efficiently demonstrating its more excellent capability for disturbance rejection.

8.4.3. *Input voltage fluctuation*

Similar to disturbance introduced in load voltage in the previous section, the fluctuations were also created between $t = 2$ *s* and $t = 4$ *s* in the input voltage, as well, and the output voltage performance of the proposed IHGS-FOPID controller was analyzed comparatively. Fig. 12 demonstrates the comparative performance of different methods in terms of dealing such a disturbance in the input voltage. As is the case for the external disturbance shown in the previous section, the proposed IHGS-FOPID controller perform more excellently to eliminate the effect of such fluctuations further confirming its good capability.

8.4.4. *Measurement noise*

To evaluate the performance of the proposed method in terms of suppression of the measurement noise, a white Gaussian noise was modeled in this study by selecting the signal-to-noise ratio (*SNR*) as 20 *dB*. The comparative results for different methods against measurement noise are provided in Fig. 13. As shown in the latter figure, the proposed IHGS-FOPID controller for the buck converter system deals with the noise more efficiently and reaches the most optimal dynamic response further confirming the robust structure of the proposed approach.

8.5. *Comparison with the state-of-the-art approaches*

This paper lastly evaluates the performance of the proposed IHGS-FOPID controller for the buck converter system comparatively by employing other best performing and available approaches reported for the same buck converter system in the literature. In this regard, particle swarm optimization (PSO), artificial bee colony (ABC), LFD and the LFD with simulated annealing (LFDSA) based FOPID controllers [8]; manta ray foraging optimization (MRFO), arithmetic optimization algorithm (AOA) and modified LFD (mLFD) based PIDA controllers [7]; PSO, differential evolution (DE) and AEO with Nelder-Mead (NM) based PID controllers [6]; HHO based PID controller [18]; genetic algorithm (GA) and whale optimization algorithm (WOA) based PID controllers [22]; hybrid Firefly and PSO (HFPSO) based PID controller [23] along with simulated annealing (SA) and WOA with SA (WOASAT) based PID controllers [24] were employed. Table 12 provides the comparative numerical performance analysis of the proposed IHGS-FOPID controller with respect to those listed approaches. The obtained time and

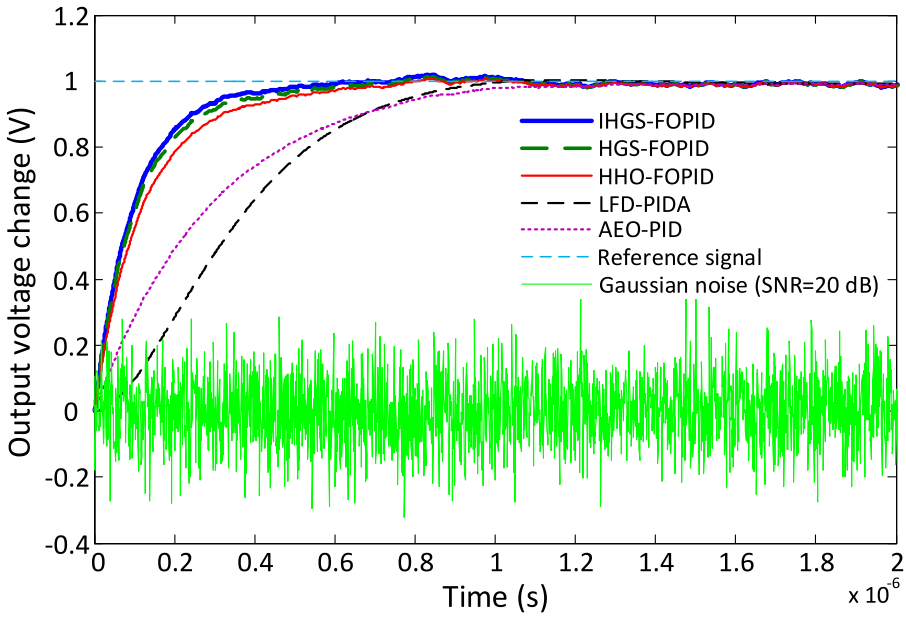


Fig. 13. Comparative performance of different methods against measurement noise.

Table 12
Comparative numerical performance analysis with respect to other available and best performing approaches in the literature.

Controller type	Overshoot (%)	Rise time (s)	Settling time (s)	Peak time (s)	Gain margin (dB)	Phase margin (deg)	Bandwidth (Hz)
IHGS-FOPID (proposed)	0	2.8510E−07	5.0765E−07	1.3686E−06	Inf.	179.9994	7.6876E+06
PSO-FOPID [8]	0	4.6066E−07	8.2062E−07	2.2108E−06	Inf.	179.9941	4.7584E+06
ABC-FOPID [8]	0	4.2808E−07	7.6297E−07	2.0539E−06	Inf.	179.9817	5.1212E+06
LFD-FOPID [8]	0	4.0260E−07	7.1709E−07	1.9322E−06	Inf.	179.9900	5.4445E+06
LFDSA-FOPID [8]	0	3.5068E−07	6.2519E−07	1.6823E−06	Inf.	179.9990	6.2520E+06
MRFO-PIDA [7]	0.0011	5.9418E−07	9.8608E−07	1.6055E−06	Inf.	178.1216	3.6190E+06
AOA-PIDA [7]	0	6.3048E−07	1.0469E−06	1.7009E−06	Inf.	175.7576	3.4110E+06
mLFD-PIDA [7]	0	5.5125E−07	9.1582E−07	1.5011E−06	Inf.	180	3.9011E+06
PSO-PID [6]	0	7.4122E−07	1.3093E−06	2.3238E−06	Inf.	177.4863	2.9515E+06
DE-PID [6]	0.0438	6.9808E−07	1.2381E−06	3.3572E−06	Inf.	178.2405	3.1369E+06
AEONM-PID [6]	0	6.1519E−07	1.0954E−06	2.9531E−06	Inf.	180	3.5628E+06
HHO-PID [18]	0	6.1087E−07	1.0876E−06	2.9324E−06	Inf.	180	3.5879E+06
GA-PID [22]	0	7.8296E−07	1.3883E−06	2.4503E−06	Inf.	178.1775	2.7966E+06
WOA-PID [22]	0	6.4306E−07	1.1391E−06	2.0134E−06	Inf.	177.9724	3.4042E+06
HFPSO-PID [23]	0.0120	6.1123E−07	1.0870E−06	2.9357E−06	Inf.	179.0014	3.5848E+06
SA-PID [24]	0.0182	7.7874E−07	1.3726E−06	2.4442E−06	Inf.	177.1461	2.8077E+06
WOASAT-PID [24]	0	6.1346E−07	1.0923E−06	2.9447E−06	Inf.	180	3.5728E+06

frequency related performance metrics clearly shows the greater capacity of the proposed method in terms of efficient operation of the buck converter system.

9. Conclusion

A novel method is proposed in this paper to design an efficient FOPID controlled buck converter system. In this regard, an improved version of the HGS algorithm is constructed with the aid of the NMS and RLM techniques. More excellent intensification and diversification capabilities of the developed IHGS algorithm are demonstrated comparatively using twenty-three classical unimodal, multimodal, and fixed dimensional benchmark functions together with the challenging CEC2019 test suite. A modified version of ISE performance index is also proposed as a novel objective function in this paper in order to allow reaching the optimal parameters of the FOPID controller employed in a buck converter system. The proposed method is comparatively demonstrated to be a more efficient design approach to tune a FOPID controlled buck converter system. Several analyses such as transient and frequency response characteristics together with the robustness, in terms of parametric uncertainties and measurement noise along with input and load voltage fluctuations, are performed against different types of the controllers tuned with recent and good performing metaheuristic algorithms (HHO-FOPID [18], LFD-PIDA [7] and AEO-PID [6]) in order to demonstrate the superiority of the proposed IHGS-FOPID approach for operating a buck converter system. The other reported and capable approaches (PSO-FOPID, ABC-FOPID, LFD-FOPID and LFDSA-FOPID [8]; MRFO-PIDA, AOA-PIDA and mLFD-PIDA [7]; PSO-PID, DE-PID, and AEONM-PID [6]; HHO-PID [18]; GA-PID and WOA-PID [22]; HFPSO-PID [23]; SA-PID and WOASAT-PID [24]) reported in literature are also used to further confirm the excellent capacity of the proposed IHGS-FOPID for controlling a buck converter system.

Declaration of Competing Interest

All authors declare that they have no conflict of interest.

References

[1] S.A. Saadat, S.M. Ghamari, H. Mollaee, Adaptive backstepping controller design on Buck converter with a novel improved identification method, IET Control Theory Appl. 16 (2022) 485–495, https://doi.org/10.1049/cth2.12241.

[2] G. Zhang, Z. Li, B. Zhang, W.A. Halang, Power electronics converters: past, present and future, Renew. Sustain. Energy Rev. 81 (2018) 2028–2044, https://doi.org/10.1016/j.rser.2017.05.290.
[3] C. Wu, F. Blaabjerg, Advanced control of power electronic systems—An overview of methods. Blaabjerg FBT-C of PEC and S (ed) Control of Power Electronic Converters and Systems, Elsevier, 2021, pp. 1–33.
[4] S.M. Ghamari, H.G. Narm, H. Mollaee, Fractional-order fuzzy PID controller design on buck converter with antlion optimization algorithm, IET Control Theory Appl. 16 (2022) 340–352, https://doi.org/10.1049/cth2.12230.
[5] P. Warrier, P. Shah, Optimal fractional PID controller for buck converter using cohort intelligent algorithm, Appl. Syst. Innov. 4 (2021) 50, https://doi.org/10.3390/asi4030050.
[6] D. Izci, B. Hekimoğlu, S. Ekinci, A new artificial ecosystem-based optimization integrated with Nelder-Mead method for PID controller design of buck converter, Alexand. Eng. J. 61 (2022) 2030–2044, https://doi.org/10.1016/j.aej.2021.07.037.
[7] D. Izci, S. Ekinci, B. Hekimoğlu, A novel modified Lévy flight distribution algorithm to tune proportional, integral, derivative and acceleration controller on buck converter system, Trans. Inst. Meas. Control 44 (2022) 393–409, https://doi.org/10.1177/01423312211036591.
[8] D. Izci, S. Ekinci, B. Hekimoğlu, Fractional-order PID controller design for buck converter system via hybrid Lévy flight distribution and simulated annealing algorithm, Arab. J. Sci. Eng. (2022), https://doi.org/10.1007/s13369-021-06383-z.
[9] S.M. Ghamari, H. Mollaee, F. Khavari, Robust self-tuning regressive adaptive controller design for a DC–DC BUCK converter, Measurement 174 (2021), 109071, https://doi.org/10.1016/j.measurement.2021.109071.
[10] O. Kaplan, F. Bodur, Second-order sliding mode controller design of buck converter with constant power load, Int. J. Control (2022) 1–17, https://doi.org/10.1080/00207179.2022.2037718.
[11] N. Snehal, W. Pooja, K. Sonam, Model predictive control for DC-DC buck converter using enumeration, in: 2020 52nd North American Power Symposium (NAPS). IEEE, 2021, pp. 1–6.
[12] A. Ghosh, M. Prakash, S. Pradhan, S. Banerjee, A comparison among PID, Sliding Mode and internal model control for a buck converter, in: IECON 2014 - 40th Annual Conference of the IEEE Industrial Electronics Society, IEEE, 2014, pp. 1001–1006.
[13] P. Shah, S. Agashe, Review of fractional PID controller, Mechatronics 38 (2016) 29–41, https://doi.org/10.1016/j.mechatronics.2016.06.005.
[14] C.A. Monje, B.M. Vinagre, V. Feliu, Y. Chen, Tuning and auto-tuning of fractional order controllers for industry applications, Control Eng. Pract. 16 (2008) 798–812, https://doi.org/10.1016/j.conengprac.2007.08.006.
[15] A. Tepljakov, B.B. Alagoz, C. Yeroglu, et al., FOPID controllers and their industrial applications: a survey of recent results, IFAC-PapersOnLine 51 (2018) 25–30, https://doi.org/10.1016/j.ifacol.2018.06.014.
[16] A. Thangaraj, S.A.E. Xavier, P. Ramasamy, An EGA approach-based fractional order PID controller for synchronous buck converters, J. Circuit. Syst. Comput. 30 (2021), 2150253, https://doi.org/10.1142/S0218126621502534.
[17] D. Izci, S. Ekinci, H.L. Zeynelgil, J. Hedley, Fractional order PID design based on Novel improved slime Mould algorithm, Electr. Power Comp. Syst. (2022) 1–18, https://doi.org/10.1080/15325008.2022.2049650.
[18] S. Ekinci, B. Hekimoglu, A. Demiroren, S. Kaya, Harris hawks optimization approach for tuning of FOPID controller in DC-DC buck converter, in: 2019 International Artificial Intelligence and Data Processing Symposium (IDAP). IEEE, 2019, pp. 1–9.
[19] Y. Yang, H. Chen, A.A. Heidari, A.H. Gandomi, Hunger games search: visions, conception, implementation, deep analysis, perspectives, and towards performance shifts, Expert Syst. Appl. 177 (2021), 114864, https://doi.org/10.1016/j.eswa.2021.114864.
[20] J.A. Nelder, R. Mead, A simplex method for function minimization, Comput. J. 7 (1965) 308–313, https://doi.org/10.1093/comjnl/7.4.308.
[21] B. Yan, Z. Zhao, Y. Zhou, et al., A particle swarm optimization algorithm with random learning mechanism and Levy flight for optimization of atomic clusters, Comput. Phys. Commun. 219 (2017) 79–86, https://doi.org/10.1016/j.cpc.2017.05.009.
[22] B. Hekimoglu, S. Ekinci, S. Kaya, Optimal PID controller design of DC-DC buck converter using whale optimization algorithm, in: 2018 International Conference on Artificial Intelligence and Data Processing (IDAP), IEEE, 2018, pp. 1–6.
[23] S. Ekinci, B. Hekimoglu, E. Eker, D. Sevim, Hybrid firefly and particle Swarm optimization algorithm for PID controller design of buck converter, in: 2019 3rd International Symposium on Multidisciplinary Studies and Innovative Technologies (ISMSIT). IEEE, 2019, pp. 1–6.
[24] B. Hekimoglu, S. Ekinci, Optimally designed PID controller for a DC-DC buck converter via a hybrid whale optimization algorithm with simulated annealing, Electrica 20 (2020) 19–27, https://doi.org/10.5152/electrica.2020.19034.
[25] K. Smedley, S. Cuk, Switching flow-graph nonlinear modeling technique, IEEE Trans. Power Electron. 9 (1994) 405–413, https://doi.org/10.1109/63.318899.
[26] B.C. Kuo, Automatic Control Systems, 8th ed., John Wiley & Sons, New York, 2003.
[27] V.A. S, T. Ananthan, FOPID controller for buck converter, Procedia Comput. Sci. 171 (2020) 576–582, https://doi.org/10.1016/j.procs.2020.04.062.
[28] M. Micev, M. Ćalasan, D. Oliva, Fractional order PID controller design for an AVR system using Chaotic Yellow Saddle Goatfish algorithm, Mathematics 8 (2020) 1182, https://doi.org/10.3390/math8071182.
[29] I. Petráš, Tuning and implementation methods for fractional-order controllers, Fract. Calc. Appl. Anal. 15 (2012) 282–303, https://doi.org/10.2478/s13540-012-0021-4.
[30] D. Cafagna, Fractional calculus: a mathematical tool from the past for present engineers [Past and present], IEEE Ind. Electron. Mag. 1 (2007) 35–40, https://doi.org/10.1109/MIE.2007.901479.
[31] M. Ausloos, M. Dirickx, The Logistic Map and the Route to chaos: From the Beginnings to Modern Applications, Springer Science & Business Media, 2006.
[32] A. Oustaloup, F. Levron, B. Mathieu, F.M. Nanot, Frequency-band complex noninteger differentiator: characterization and synthesis, IEEE Trans. Circuit. Syst. I Fundam. Theory Appl. 47 (2000) 25–39, https://doi.org/10.1109/81.817385.
[33] D. Izci, S. Ekinci, E. Eker, M. Kayri, A novel modified opposition-based hunger games search algorithm to design fractional order proportional-integral-derivative controller for magnetic ball suspension system, Adv. Control Appl. 4 (2022) e96, https://doi.org/10.1002/adc2.96.
[34] S. Ekinci, D. Izci, B. Hekimoğlu, Optimal FOPID speed control of DC motor via opposition-based hybrid manta ray foraging optimization and simulated annealing algorithm, Arab. J. Sci. Eng. 46 (2021) 1395–1409, https://doi.org/10.1007/s13369-020-05050-z.
[35] A. Demirören, S. Ekinci, B. Hekimoğlu, D. Izci, Opposition-based artificial electric field algorithm and its application to FOPID controller design for unstable magnetic ball suspension system, Eng. Sci. Technol. an Int. J. 24 (2021) 469–479, https://doi.org/10.1016/j.jestch.2020.08.001.



Davut Izci received his BSc degree from Dicle University, Turkey, in Electrical and ElectronicEngineering and his MSc and PhD degrees from Newcastle University, England - UK, in Mechatronics and Microsystems, respectively. He is currently an Assistant Professor working at Batman University, Turkey. He carries out teaching and research activities both in Faculty of Engineering and Vocational School of Technical Sciences. His-research interests are in microsystems development, sensing applications, robotics, and the applications of meta-heuristic optimization algorithms to various control systems.



Serdar Ekinci received his BSc degree in Control Engineering, and his MSc and PhD degrees in Electrical Engineering all from Istanbul Technical University (ITU), in 2007, 2010 and 2015, respectively. He is currently an Associate Professor working in Department of Computer Engineering at Batman University, Turkey. His-areas of interest are electrical power system, stability, control technology and the applications of metaheuristic optimization algorithms to various control systems.